PNAS RESEARCH ARTICLE | ENGINEERING

Ultrasensitive and ultrastretchable electrically self-healing conductors

Yanyan Li[a,b,c,1], Ting Fang[a,b,c,1], Jiaxue Zhang[a,b,c], Hangyu Zhu[a,b,c], Yuping Sun[a,b,c], Shaolei Wang[a,b,c], Yanqing Lu[a,d,2], and Desheng Kong[a,b,c,2]

Edited by Yonggang Huang, Northwestern University, Glencoe, IL; received January 18, 2023; accepted April 28, 2023

Self-healing is a bioinspired strategy to repair damaged conductors under repetitive wear and tear, thereby largely extending the life span of electronic devices. The self-healing process often demands external triggering conditions as the practical challenges for the widespread applications. Here, a compliant conductor with electrically self-healing capability is introduced by combining ultrahigh sensitivity to minor damages and reliable recovery from ultrahigh tensile deformations. Conductive features are created in a scalable and low-cost fabrication process comprising a copper layer on top of liquid metal microcapsules. The efficient rupture of microcapsules is triggered by structural damages in the copper layer under stress conditions as a result of the strong interfacial interactions. The liquid metal is selectively filled into the damaged site for the instantaneous restoration of the metallic conductivity. The unique healing mechanism is responsive to various structural degradations including microcracks under bending conditions and severe fractures upon large stretching. The compliant conductor demonstrates high conductivity of ~12,000 S/cm, ultrahigh stretchability of up to 1,200% strain, an ultralow threshold to activate the healing actions, instantaneous electrical recovery in microseconds, and exceptional electromechanical durability. Successful implementations in a light emitting diode (LED) matrix display and a multifunctional electronic patch demonstrate the practical suitability of the electrically self-healing conductor in flexible and stretchable electronics. The developments provide a promising approach to improving the self-healing capability of compliant conductors.

self-healing | stretchable conductor | liquid metal | stretchable electronics | flexible conductor

Significance

Bio-inspired self-healing conductors may significantly extend the service life of electronic devices. The promising potentials are often challenged by slow and nonspontaneous reparation processes demanding external triggering conditions. We have introduced an innovative design of self-healing conductors with extremely low thresholds to restore electrical properties. The healing mechanism applies to different levels of structural damages from tiny microcracks to severe fractures. Our work advances electrically self-healing conductors to enable robust device performances in flexible and stretchable electronics.

Conventional electronics are driven by the constant pursuit of improved processing speed and energy efficiency. The rapid developments of flexible electronic devices offer a new paradigm of technology highlighting lightweight design, scalable fabrication, and structural adaptability (1–3). The rollable and foldable forms of electronic gadgets allow convenient carry around and interface with complex geometry (4). The recent emergence of stretchable devices further expands the mechanical deformability toward twisting, stretching, and compressing (5, 6). The conformal integration of stretchable electronic devices with the soft and curvilinear human body is the enabler of promising applications in advanced prosthetics (6, 7), health-care monitoring (8–10), and human–machine interfaces (11, 12). Compliant conductors represent indispensable material components for active electrodes and electronic interconnects, which are created by engineering designs, ultrathin layouts, and the addition of soft polymers (13). In spite of the substantially improved mechanical deformability, the compliant conductors are still vulnerable to structural degradations in terms of cracks and delamination by repetitive wear and tear (14). The spontaneous suppression of these failure mechanisms is therefore essential for the stable operation of flexible and stretchable electronics during long-term practical applications.

To this end, the biological system has an alternative survival strategy featuring autonomous recovery from unexpected damages. The self-healing capability has already been explored as a promising approach to largely extend the service life of functional devices and systems (15, 16). Intrinsically self-healing conductors are typically formed by filling metallic nanostructures into soft polymers with abundant reversible bonds, which allows the reparation of the damaged conductive network through the reconstruction of the polymer matrix (17–20). In response to the practical challenge of autonomous recovery under ambient conditions, a variety of approaches have already been explored to accelerate the healing speed in terms of elevated temperatures, photo-irradiations, and solvent vapor exposures (20). In contrast, extrinsically self-healing polymer composites rely on embedded microcapsules containing reactive precursors and catalysts, which are released by external damages to induce autonomous recovery through polymerization reactions (21, 22). The mechanism unfortunately prohibits repetitive healing processes at the same location due to the consumption of the healing agents (15).

Author affiliations: [a]College of Engineering and Applied Sciences, National Laboratory of Solid State Microstructure, and Collaborative Innovation Center of Advanced Microstructures, Nanjing University, Nanjing 210093, China; [b]State Key Laboratory of Analytical Chemistry for Life Science, Nanjing University, Nanjing 210023, China; [c]Jiangsu Key Laboratory of Artificial Functional Materials, Nanjing University, Nanjing 210023, China; and [d]Key Laboratory of Intelligent Optical Sensing and Manipulation, Nanjing University, Nanjing 210093, China

Author contributions: Y. Lu and D.K. designed research; Y. Li, T.F., J.Z., H.Z., Y.S., and S.W. performed research; Y. Lu contributed new reagents/analytic tools; Y. Li and T.F. analyzed data; and Y. Li and D.K. wrote the paper.

The authors declare no competing interest.

This article is a PNAS Direct Submission.

[1]Y.L. and T.F. contributed equally to this work.

[2]To whom correspondence may be addressed. Email: yqlu@nju.edu.cn or dskong@nju.edu.cn.

This article contains supporting information online at https://www.pnas.org/lookup/suppl/doi:10.1073/pnas.2300953120/-/DCSupplemental.

Published May 30, 2023.

Gallium-based alloys, commonly termed as liquid metals, have emerged as a class of distinctive healing reagents featuring metallic conductivity and liquid-phase deformability (23–26). Liquid metal microcapsules are top-down synthesized from bulk alloys with native oxides or coordinating ligands as the stabilizing shell (27–29). Instead of rejuvenating the polymer matrix, the released liquid metal serves as the electrical rejuvenator for the lost conductive pathways (30–32). Liquid metal microcapsules typically form insulating composites with polymers as a result of the passivating shells to hinder the charge transport. The sintering procedures are necessary to merge the microcapsules for effective conductivity by way of strong compression or large tensile strains (30, 33, 34), thereby further increasing the overall complexity of the fabrication process. Conductive self-healing composites are created by introducing additional metallic fillers to establish three-dimensional percolation network (32, 35). Despite the excellent performance under large strains, the composite lacks the triggering mechanism to activate the healing capability under minor deformations (32, 35). Large resistance fluctuations are commonly encountered during repetitive deformations due to the weak interactions between the liquid metal microcapsules and conductive fillers. An alternative design of self-healing conductor is prepared by drop casting liquid metal microcapsule ink on top of metal films (31, 36). The electrical restoration requires deep cut across the entire composite to ensure the effective release of liquid metal at the damaged site, largely limiting the application settings to special circumstances involving catastrophic structural failures.

In this study, we report the design and fabrication of an electrically self-healing conductor featuring ultrahigh sensitivity to tiny damages and adaptability to giant deformations. The conductor has a unique architecture comprising a copper layer strongly coupled with underlying liquid metal microcapsules. These microcapsules are directly ruptured by any structural damages generated in the copper layer under bending, folding, and stretching conditions. The selective release of liquid metal to damaged sites allows the instantaneous recovery of the excellent conductivity of ~12,000 S/cm. The unique healing mechanism is extremely sensitive to microcracks in the copper layer generated under a tiny bending strain of 0.25%. The strategy also allows the conductor to withstand severe fractures at an ultrahigh tensile strain of 1,200%. The self-healing conductor retains robust electrical properties under various mechanical manipulations, which are demonstrated by durable devices including a flexible LED matrix display and a skin-attachable electronic patch. The design strategy reported here provides an attractive avenue to enhance the electrically self-healing capability of compliant conductors.

Results and Discussion

Design and Preparation of Electrically Self-Healing Conductors. As schematically illustrated in Fig. 1*A*, the electrically self-healing conductor exhibits a bilayer architecture comprising a conductive copper layer on top of liquid metal microcapsules. Cracks in the Cu layer are generated as the major degradation mechanism under stress conditions during long-term practical applications (20). Liquid metal microcapsules are punctured by the tip-stress field of the cracks along the propagation paths due to the strong interfacial coupling with the Cu layer (37, 38). The released liquid metal recovers the electrical properties by reestablishing the lost conducting pathways in the fractured Cu conductor. A top-down, high-yield synthesis utilizes ultrasonication to create liquid metal/fatty acid core-shell microcapsules with controlled sizes (*SI Appendix*, Fig. S1) (33). A viscous ink is formulated by mixing 2.8 μm-sized microcapsules and a styrene–isoprene–styrene (SIS) elastomer in toluene solution. In Fig. 1*B*, screen printing is employed as a scalable approach to create arbitrary patterns as exemplified by the flower feature in metallic gray color. The printed composite is an electrical insulator consisting of isolated liquid metal microcapsules, as shown by scanning electronic microscopy (SEM) image in Fig. 1*C*. In a chemical bath, a galvanic displacement reaction selectively generates Cu seeds over liquid metal microcapsules (39, 40), thereby promoting the subsequent electroless deposition of the Cu layer. The printed liquid metal microcapsules therefore serve as the template for the bilayer conductor. The overall process allows the scalable fabrication of delicate conductive features with a resolution of 50 μm (*SI Appendix*, Figs. S2 and S3). In Fig. 1*C*, SEM image reveals the conformal deposition of the copper layer over liquid metal microcapsules to establish the strong interfacial interactions.

The electrically self-healing conductor has compliant mechanical properties (*SI Appendix*, Fig. S4). In Fig. 1*D*, a representative conductor is evaluated by cyclic tensile deformations, with the peak strain progressively increasing from 3 to 50%. The resistance exhibits steady increases upon stretching and almost full recovery after relaxation to demonstrate robust electrical properties. The behavior is in sharp contrast to the completely lost conductivity of regular copper films at a tiny strain of ~3%, as shown in *SI Appendix*, Fig. S5. The conductor is immune to electrical failures by spontaneously repairing any damages in the conductive copper layer. The electrically self-healing capability is not the inherent property of the liquid metal microcapsules. As-printed microcapsules require a large activation strain of ~30% to release sufficient liquid metal for an interconnect conductive network (32, 41), as exemplified in *SI Appendix*, Fig. S6. The bilayer architecture effectively lowers the triggering threshold for electrical restorations.

Microstructure characterizations provide insights into the healing mechanism. In Fig. 1*E*, the copper film is mechanically brittle and readily fractured at 3% strain. In the electrically self-healing conductor, the damage in the copper layer follows a similar trend likely due to the compliant nature of liquid metal microcapsules. Due to the robust interfacial coupling, the liquid metal microcapsules are ruptured by the stress field of copper film microcracks to achieve the selective release of a large amount of healing agent at the damage site (Fig. 1*E* and *SI Appendix*, Fig. S7). A remarkable observation is the spontaneous filling of liquid metal into the cracks immediately following their formations according to Movie S1. The unique phenomenon is responsible for the ultrasensitive reparation of minute electrical damages under low tensile strains. The instantaneous completion of the healing process within a few microseconds further enables the real-time restoration of the electrical properties as illustrated in *SI Appendix*, Fig. S8. In comparison, as-printed liquid metal microcapsules are randomly ruptured to release the encased conductor upon tensile deformations (Fig. 1*C* and *SI Appendix*, Fig. S9). Conventional liquid metal–based conductors have demanding triggering conditions largely due to the random sintering process as an inefficient healing mechanism.

In addition, the fragmentation process of the copper layer upon stretching has been quantitatively analyzed as shown in Fig. 1*F*. The initial regime is dominated by the generation of microcracks with the Cu domain size (42). The crack width shows slow increases with the strain. The embedded microcapsules are ruptured along the crack propagations for the spontaneous release of the liquid metal. As the strain increases above ~25%, the tensile deformation is primarily accommodated by the expanded cracks due to the reduced stress transfer to the Cu layer (43). The

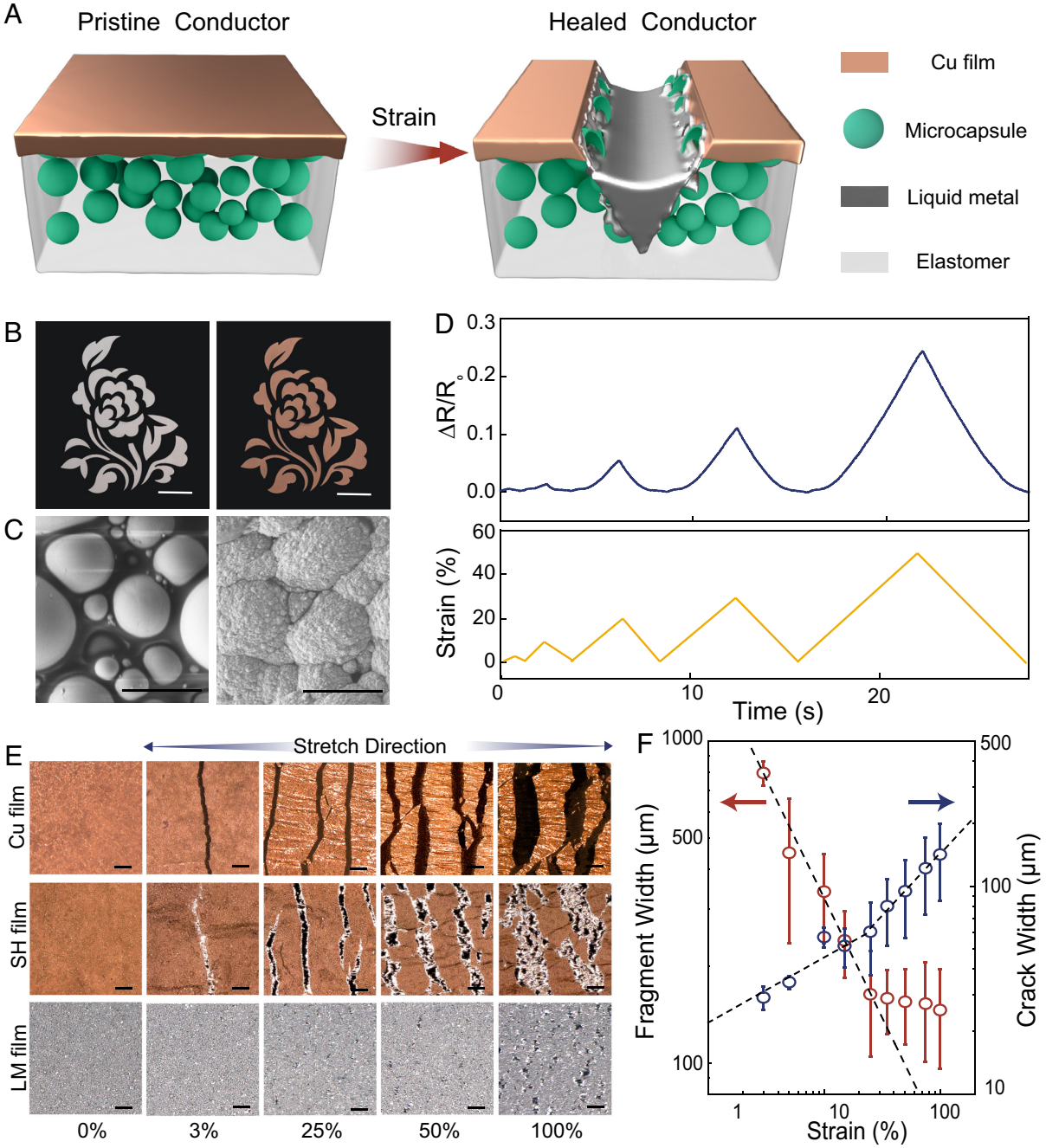

Fig. 1. Design and preparation of the self-healing conductor. (*A*) Schematic illustration of the ultrasensitive self-healing mechanism. (*B*) Optical images showing a flower-shaped pattern of screen-printed liquid metal microcapsules before (*Left*) and after (*Right*) the electroless deposition process. (Scale bars: 1 cm.) (*C*) SEM images acquired before (*Left*) and after (*Right*) the electroless deposition process. (Scale bars: 5 μm.) (*D*) Normalized resistance of the self-healing conductor under stretch–relaxation cycles to varying tensile strains. (*E*) Optical microscopy images revealing the microstructure evolutions at different tensile strains for a copper film (*Top*), a self-healing conductor (*Middle*), and a liquid metal microcapsule composite (*Bottom*). (Scale bars: 100 μm.) (*F*) Quantitative structural analysis on the fractured Cu layer in the self-healing conductor.

inhomogeneous strain distribution promotes the selective mechanical sintering of additional liquid metal microcapsules to replenish the widened cracks (41, 44). The strongly coupled conductive layer with liquid metal microcapsules is essential for the universal healing capability applicable to various structural damages through the self-adaptive release of the healing agent.

Attractive Physical Properties. The as-prepared conductor has the characteristic reddish-orange color of copper, as shown in Fig. 2 *A*, *Inset*. A gradual color shift to silvery white is observed in response to large tensile deformations of up to 1,200% strain. In Fig. 2*A*, the resistance of the electrically self-healing conductor exhibits stable and limited increases upon stretching. Specifically, the normalized resistance is 1.5 at 100% strain, 5.7 at 400% strain, and 38.1 at 1,200% strain. The resistance almost returns to the original value with a minor irreversible change of ~30% after releasing the tensile strain. In Fig. 2*B*, the optical microscopy image reveals the continuous expansion of the cracks under the enormous tensile strains. The fractured copper layer is interconnected by soft liquid metal joints to retain electrical stability. In spite of tensile deformations and relaxations, the liquid metal is stabilized by native oxides to avoid any obvious spread (45), as shown in *SI Appendix*, Fig. S10. The conductor is further examined by tensile fatigue tests with different strain levels

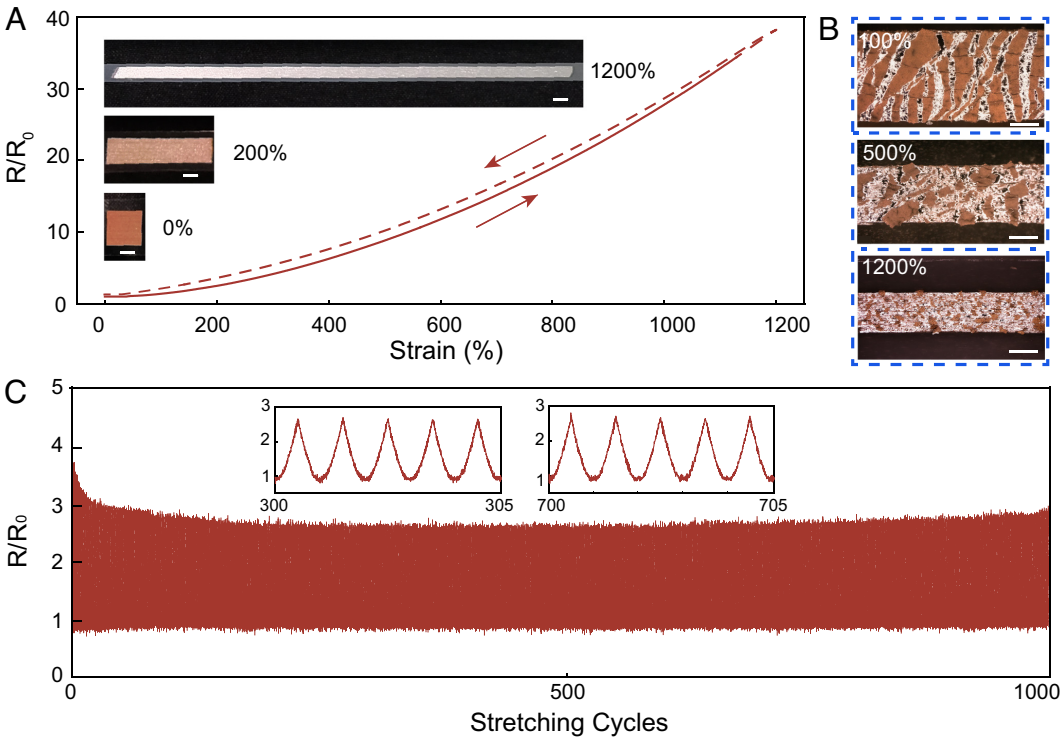

Fig. 2. Ultrastretchable self-healing conductors. (*A*) Normalized resistance versus tensile strain during loading–unloading to 1,200% strain. (*Inset*) Optical images of the self-healing conductor in the strain range from 0 to 1,200%. (Scale bars: 1 cm.) (*B*) Optical microscopy images of the self-healing conductor under different tensile strains. (Scale bars: 500 μm.) (*C*) Change in resistance over 1,000 stretch–relaxation cycles to 300% strains. (*Inset*) Normalized resistance at 301st to 305th and 701st to 705th cycles.

(Fig. 2*C* and *SI Appendix*, Fig. S11). A relatively stable resistance is preserved during 1,000 stretch–relaxation cycles to 300% strain, as shown in Fig. 2*C*, thereby confirming the electromechanical durability for long-term practical applications. In the initial cycles, the minor increase of the resistance at the relaxed state is likely associated with the irreversible elongation of the SIS substrate (*SI Appendix*, Fig. S12). Apart from tensile deformations, the conductor is sufficiently robust to withstand decent compressive loads of up to 1.5 MPa. The liquid metal is filled into emerging cracks of the Cu layer without any noticeable overspill, as shown in *SI Appendix*, Fig. S13. The electrically self-healing capability also applies to a wide range of temperatures from −15 °C to 80 °C (*SI Appendix*, Fig. S14). In addition, the conductor has excellent environmental stability to allow long-term storage under ambient conditions (*SI Appendix*, Fig. S15). Interestingly, the high conductivity and stretchability are negligibly affected by the storage in an aqueous environment, as shown in *SI Appendix*, Fig. S16. The stable properties of the electrically self-healing conductor may expand the scope of the potential application settings.

Influences of the Copper Layers. The Cu layer is electrolessly deposited to provide the original conductivity. The Cu mass density increases with the deposition duration, as shown in *SI Appendix*, Fig. S17. In Fig. 3*A*, the nominal conductivity of the electrically self-healing conductor is positively correlated with the deposition time. Specifically, the conductivity value reaches 6.1×10^3 S/cm at 30 min, 1.2×10^4 S/cm at 40 min, and 2.5×10^4 S/cm at 60 min. The self-healing capability is explored by inducing extensive structural damages under uniaxial tensile deformation of 300% strain. The healed conductor at the relaxed condition exhibits enhanced conductivity for short electroless depositions and lowered conductivity for lengthy depositions (Fig. 3*B*). A rough compensation is achieved at an intermediate deposition duration of 40 min, generating ~1.5 μm-thick copper layer over 25 μm-thick liquid metal microcapsules (*SI Appendix*, Fig. S18). The condition is therefore adopted in most experiments with the optimal recovery rate. In Fig. 3*C*, the healing capability is also correlated with the level of structural damage. The healed resistance initially drops by increasing the experienced tensile strain as released liquid metal overcompensates for lost conducting pathways. The healed resistance switches to a rising trend for experienced tensile deformations above 400% strain. The increase in the resistance is ascribed to the irreversible elongation of the elastomer substrate after large tensile strains (*SI Appendix*, Fig. S19). The conductor demonstrates fairly stable resistance within 40% variations for tensile strains of up to 1,200%, representing universal healing capability to withstand large loadings and unexpected impacts in practical applications. The behavior contrasts sharply with liquid metal microcapsule composites exhibiting strain-dependent resistance (*SI Appendix*, Fig. S20). Additionally, the Cu layer allows an alternative deposition method through thermal evaporation. In *SI Appendix*, Fig. S21, a 250-nm-thick Cu layer on liquid metal microcapsules retains excellent self-healing behavior of electrical properties, demonstrating the general applicability of the bilayer architecture.

Influences of the Liquid Metal Microcapsule Composites. The liquid metal microcapsules are the healing agents for electrically self-healing conductors. The ultrasonication time is the effective knob to control the dimension of liquid metal microcapsules, as illustrated in *SI Appendix*, Fig. S22. Large microcapsules of 11.6 ± 5.1 μm lead to poor printing quality with highly textured surfaces. Liquid metal microcapsules with reduced dimensions are well suited for generating dense, pinhole-free composite layers. In *SI Appendix*, Fig. S23, the corresponding conductor based on ultrafine microcapsules of 0.9 ± 0.5 μm cannot fully recover

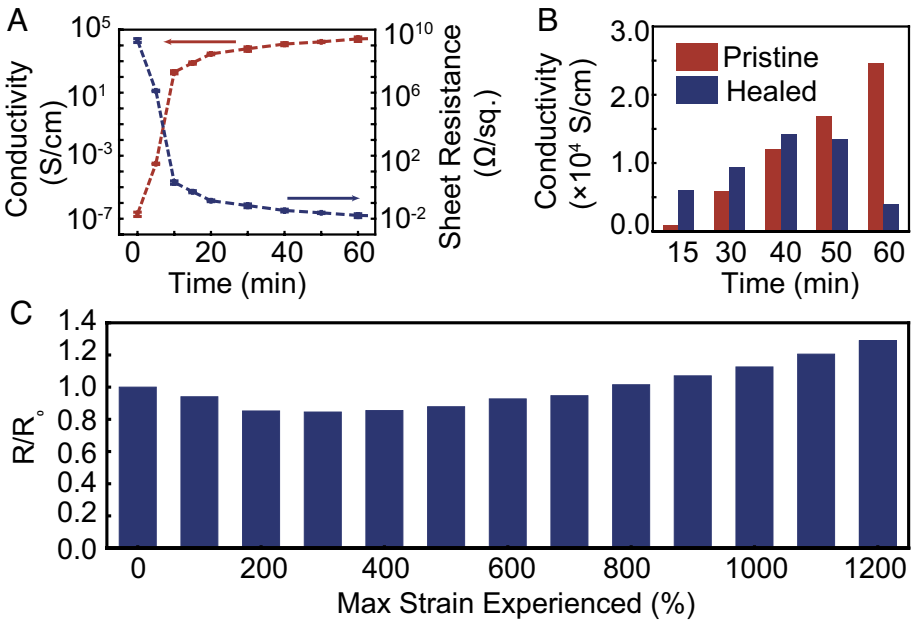

Fig. 3. Influence of the electroless deposition condition on the self-healing conductor. (*A*) Conductivity and sheet resistance of the self-healing conductors based on different deposition durations. (*B*) Conductivity at pristine and healed conditions. The conductors undergo 300% tensile strain to induce extensive structural damage. (*C*) Normalized resistance of the healed conductor after experiencing different levels of tensile deformations.

the original electrical properties after tensile deformations, likely associated with the inverse correlation of the rupture pressure on the microcapsule diameter (46). Accordingly, the optimal choice is liquid metal microcapsules in 2.8 ± 1.8 μm. In addition, SIS binder concentration is also critical for liquid metal microcapsule composites. As illustrated in *SI Appendix*, Fig. S24, additional liquid metal microcapsules are exposed on the composite layer by reducing the binder, thereby accelerating the deposition rate of the copper film. The corresponding conductor exhibits improved electromechanical properties by facilitating stress transfer onto liquid metal microcapsules (44). However, inks with insufficient binders tend to print low-quality features with excessive cracks. A weight ratio 2:50 between SIS binder and liquid metal microcapsules effectively balances printability and healing capability.

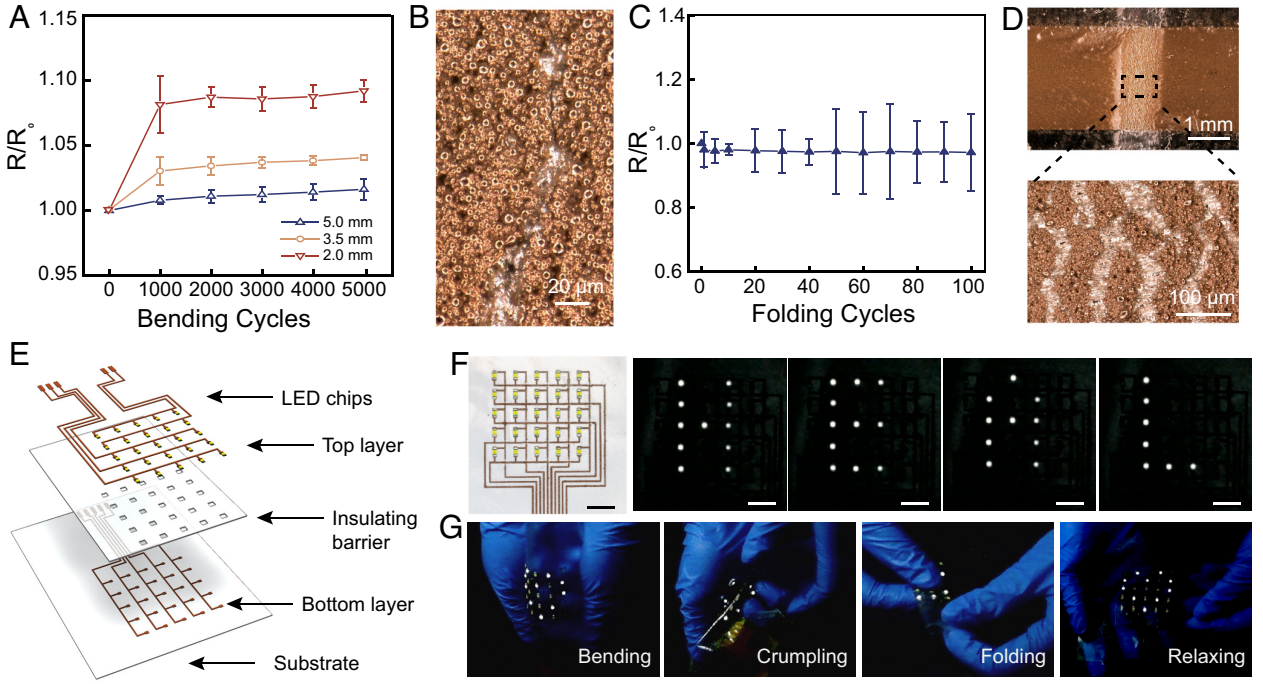

Fig. 4. Implementation of self-healable conductors in flexible electronic devices. (*A*) Change in resistance of the self-healing conductor over 5,000 bending cycles to different radii. (*B*) Optical microscopy image captured after the cycling with a radius of 2.0 mm. (*C*) Change in resistance over 100 folding cycles. (*D*) Optical microscopy images revealing the microstructure of the crease on the cycled conductor. (*E*) Schematic showing the layer-by-layer architecture of the flexible LED matrix display. (*F*) Optical images of an as-prepared LED matrix to display different alphabets. (Scale bars: 1 cm.) (*G*) Mechanical manipulations of an LED matrix displaying a heart-shaped pattern.

Electrically Self-Healing Conductors for Flexible Electronics. The electrically self-healing conductor represents an attractive candidate material to increase the life span of flexible electronic devices. To evaluate the mechanical flexibility, the as-prepared conductor on the polyethylene terephthalate (PET) substrate is repetitively actuated between the flat and outward bending states using a motorized translational stage. The resistance versus the number of bending cycles is shown in Fig. 4*A*. The conductor retains robust electrical properties over 5,000 cycles with different bending radii from 2 to 5 mm. In spite of some microcracks as shown in Fig. 4*B*, the conductor retains the conducting pathways through the on-demand release of liquid metal at the damaged site. The healing capability, therefore, exhibits ultrahigh sensitivity to minor injuries at small bending strains of down to 0.25%. In contrast to conventional mechanisms demanding external cutting or large deformations for activation, the extremely low healing threshold observed here allows the conductor to operate stably under the bending conditions. In the absence of electrical restorations, a copper film exhibits continuously increased resistance during bending fatigue tests (*SI Appendix*, Fig. S25). Additionally, the compliant conductor maintains stable resistance over 100 folding–unfolding cycles (Fig. 4*C*). In Fig. 4*D*, an optical microscopy image reveals that dense microcracks are concentrated at the crease. The exceptional resilience against mechanical folding is attributed to the electrically self-healing capability to repair the fractured copper conductive layer. As expected, the regular copper film is mechanically brittle and completely fails upon folding manipulation.

A multilayer matrix display is constructed in a layer-wise sequence by the heterogeneous interconnection of LED chips with the electrically self-healing conductor on a PET substrate, as schematically illustrated in Fig. 4*E*. In Fig. 4*F*, a representative LED display in the form of a 5 × 5 matrix allows the convenient display of variable words and graphic patterns after interfacing with an external controller (Fig. 4*F* and Movie S2). The device is sufficiently robust to retain a stable luminous pattern under various manipulations including bending, folding, and crumping, as shown in Fig. 4*G* and Movie S3. The exceptional durability is associated with the self-healing capability of the conductor to recover from accidental electrical damage.

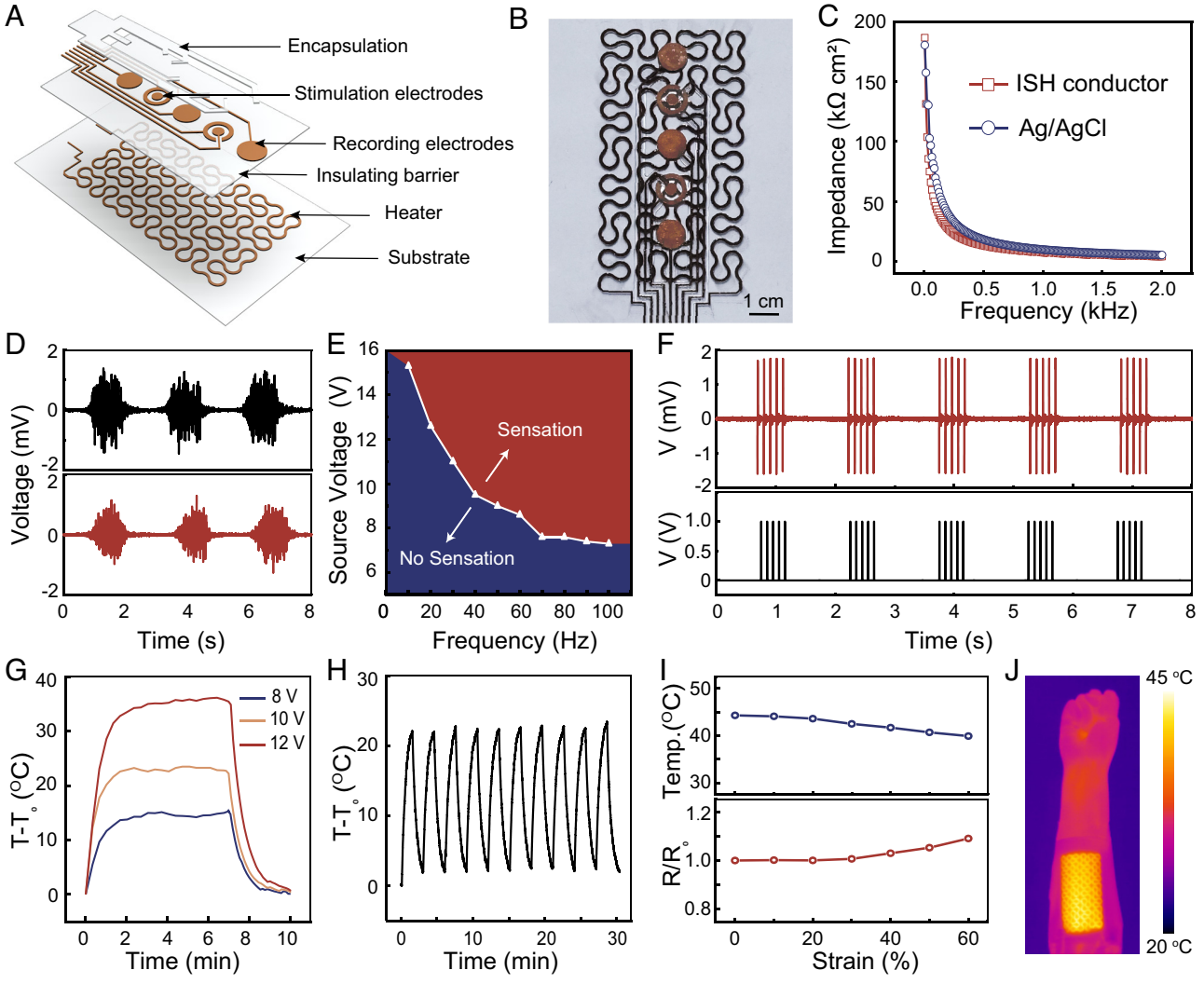

Fig. 5. Stretchable and wearable electronics based on the self-healing conductor. (*A*) Schematic illustration of the multifunctional electronic patch comprising a biopotential sensor, an electrical stimulator, and an electroresistive heater. (*B*) Optical image of an as-prepared electronic patch. (*C*) Skin contact impedance of a self-healing conductor electrode and a commercial Ag/AgCl gel electrode. (*D*) EMG signals of hand open and close gestures acquired by Ag/AgCl gel electrodes (*Top*) and self-healing conductor electrodes (*Bottom*). (*E*) Threshold voltage for perception as a function of the stimulation frequency. (*F*) EMG waveforms (*Top*) acquired during electrical stimulations with monophasic voltage pulses (*Bottom*). (*G*) Temperature profiles of the electroresistive heater under different applied voltages. (*H*) Temperature responses to on/off voltage cycles with an amplitude of 10 V. (*I*) Temperature and normalized resistance of the heaters under tensile deformations. (*J*) Infrared camera images showing the reliable heating performance of the electronic patch attached to the forearm.

Skin-Attachable Electronics Using Electrically Self-Healing Conductors. Stretchable electronics allow conformal and intimate interactions with skins for wearable sensing and simulations. The electrically self-healing conductor is highly conductive, mechanically compliant, and durable, which represents a suitable candidate material for stretchable and wearable devices. As schematically illustrated in Fig. 5*A*, a multifunctional electronic patch is composed of sensing electrodes for biopotential recording, stimulation electrodes for electrical therapy, and a heater for thermotherapy. Fig. 5*B* shows an as-prepared electronic patch which is a soft and stretchy multilayer laminate in a thin layout. The electronic patch is manually mounted on the forearm using silicone gel adhesive to achieve conformal and intimate interactions with the skin. In Fig. 5*C*, the contact impedance of the epidermal electrodes is competitive against commercial Ag/AgCl gel electrodes, which suggests the suitability for electrophysiological recording and simulation. The sensing electrodes readily capture surface electromyogram (EMG) signatures of muscle activations associated with hand open and close gestures, as shown in Fig. 5*D*. The high signal-to-noise ratio of 25.4 dB is comparable to commercial Ag/AgCl gel electrodes (26.2 dB). In addition, the electrical stimulator on the soft patch makes use of monophasic square voltage pulses to trigger subconsciously neuromuscular response, which represents an effective approach for pain relief and physical rehabilitation (47, 48). In Fig. 5*E*, the threshold voltage for perception is lowered by increasing the stimulation frequency due to the reduced contact impedance (49). In the biopotential sensor, the voltage signal shows a strong correlation with the stimulation pulses to allow simultaneous monitoring of the treatment (Fig. 5*F*). The large-area electroresistive heater allows controlled delivery of thermal stimulations. The heater exhibits fast temperature responses and durable heating performances (Fig. 5 *G* and *H*). The limited drifts in temperature upon stretching are ascribed to the negligible changes in the resistance by adopting the serpentine Peano curve design (Fig. 5*I*). Infrared camera images of the heater reveal uniform surface temperature distributions at different tensile strains (*SI Appendix*, Fig. S26). The conformal attachment of the electronic patch on the skin allows reliable heat transfer for thermal therapy (Fig. 5*J*). The combined thermal and electrical simulations are a well-recognized approach for a synergetic therapeutic outcome (48). Notice that wearable heaters of compact dimensions are also easily prepared using this fabrication strategy (*SI Appendix*, Fig. S27). In addition, the entire electronic patch is highly durable to withstand repetitive tensile deformations. All sensing and stimulation capability are well preserved after 1,000 stretch cycles to 60% strain, as shown in *SI Appendix*, Figs. S28–S30. The reliable operation is ascribed to the self-healing conductor capable of recovering from stress-induced electrical damages. Notably, the soft liquid metal joints leave no obvious residues on the skin, likely due to the passivation by native oxides (*SI Appendix*, Fig. S31).

Conclusion

In summary, we have demonstrated the universal self-healing capability of a compliant conductor suitable for minor injuries and severe fractures under various stress conditions. In a scalable fabrication process, screen-printed liquid metal microcapsules are coated with a conductive Cu layer by electroless deposition to establish strong interfacial coupling. The unique healing mechanism is associated with the rapid and efficient rupture of embedded liquid metal microcapsules by the stress field of microcracks under bending, folding, and stretching conditions. The self-adaptive release of liquid metal at the damaged locations efficiently repairs the damaged conductive layer, which is extremely sensitive to tiny microcracks and also applicable to large fractures. The compliant conductor exhibits high electrical conductivity of ~12,000 S/cm, an ultralow threshold to activate the self-healing processes, and ultrahigh deformability of up to 1,200% strain. The conductor is employed to create durable devices including an LED matrix display and a skin-attachable electronic patch. A generic design strategy is introduced here to improve the self-healing sensitivity and capability of compliant conductors, which may open up a wide range of applications in flexible and stretchable electronics.

Materials and Methods

Resource Availability. SIS (D1117) was obtained from Kraton Corporation. Liquid metal was prepared by melting a mixture of gallium, indium, and tin in a weight ratio of 68.5:21.5:10 at 80 °C for 2 h inside a glovebox. All other chemical reagents were purchased from Shanghai Macklin Biochemical Co., Ltd without further purification. Stretchable substrates were prepared by drop casting SIS solution onto octadecyltrichlorosilane-modified glass wafers and then removing the solvent.

Preparation of Printable Liquid Metal Microcapsule Ink. Liquid metal microcapsules were synthesized by adding 15 g liquid metal into 25 mL N-pentanol solution of 11-mercaptoundecanoic acid (0.25 mol L^{-1}) and then ultrasonicating at 10% power setting using a 900-W probe sonicator (ATPIO-900D, Nanjing Xianou Instrument Manufacturing Co., Ltd.). The processing duration was adjusted from 10 to 60 s to control the size of liquid metal microcapsule (*SI Appendix*, Fig. S1). As-prepared microcapsules were thoroughly washed with toluene. To prepare printable inks, a mixture of liquid metal microcapsules and SIS solution in tolune (25 wt%) was homogenized at 1,000 rpm for 20 min using a planetary mixer (JF-RVITV-150, Shenzhen Junfeng Technology Co., Ltd.). An optimized formulation was primarily used unless stated otherwise involving 2.8 μm-sized liquid metal microcapsules and SIS binder in a weight ratio of 2:50.

Preparation of the Self-Healing Conductors and Pure Copper Film. The desired features were defined on stretchable substrates using a manual screen printer (Zhuhai Kaivo Electronic Co., Ltd.) with stainless steel stencils. A copper layer was subsequently coated onto the liquid metal microcapsule pattern by chemical bath deposition carried out at 70 °C in an aqueous solution, consisting of 25.8 mM copper sulfate pentahydrate, 41.3 mM tetrasodium ethylenediaminetetraacetate dihydrate, 300 mM triethanolamine, Triton X-100 (0.1%, w/v), 0.09M sulfuric acid, and 74 mM dimethylamine borane. The copper layer thickness of the self-healing conductor was tailored by adjusting the deposition duration. A 40-min process typically yielded a coating layer of 1.5 μm in thickness. The copper film was also electrolessly deposited onto the elastomer substrate as a control following a previously reported method (50). In addition to electroless deposition, thermal evaporation was an alternative approach for ultrathin Cu films on liquid metal microcapsule composites carried out inside a high vacuum evaporator (Beijing Technol Science Co., Ltd.). The patterned films were defined by stainless-steel shadow masks.

Material Characterizations. Microstructure characterizations were performed using a Zeiss GeminiSEM 500 field emission scanning electron microscope equipped with an Oxford EDS detector. The samples were thoroughly frozen in liquid nitrogen and broken into two pieces for cross-sectional characterizations. A Keyence VHX-6000 digital microscope was used to collect optical microscopy images. Optical images and videos were taken with a Fujifilm X-T10 camera. A Keyence VK-K1000 laser scanning microscope was employed to acquire the depth profile for the thickness determination. In order to quantify the area mass density of copper, the weight change associated with copper deposition was measured using an Ohaus analytical balance (0.01 mg). The resistance was measured by using a Keithley 2634B source meter and a GWINSTEK GOM-805 milliohm meter. The electrical properties under bending and stretching deformations were evaluated on a homemade motorized linear stage. The electromechanical properties were also measured inside an environmental chamber (BPS-250CB, Shanghai Yiheng Co., Ltd.) with controlled temperatures. Mechanical properties were acquired by using a Shimadzu AGS-X universal testing machine. Uniaxial tensile measurements were carried out with 50 mm × 5 mm samples at a 50 mm/min

strain rate using a 50 N load cell. The compression loads were applied through a flat-head probe (1 cm × 1 cm) using a 1,000 N load cell. Long-term stability was evaluated by storing the samples in the environmental chamber at the ambient temperature with controlled humidity levels.

Fabrication and Evaluation for Flexible LED Arrays. A layer of conductive features in the form of interconnects is defined on a 25-μm-thick PET substrate. A layer of SIS film was screen printed over the conductive pattern for electrical insulation. A second layer of conductive pattern with interconnects and contact pads was subsequently prepared. LED chips (LTW-216TS5, 1206, Lite-On Inc.) were submerged in an acid bath (4%, w/v) to coat the contact pads with a layer of liquid metal by attaching to bulk liquid metal. Subsequently, the chips were mounted onto the contact pads and then manually pressed with a tweezer for reliable electrical connections. A layer of SIS was subsequently deposited for encapsulation based on an ultrasonic spray system operated at 40 kHz (DW-F40-60, Hangzhou Dowell Ultrasonic Technology, Co., Ltd.). A copper-clad polyimide-based flexible connector was employed to interface with an Arduino Uno microcontroller. A customized program was installed on the microcontroller to control the luminous pattern of the LED matrix display.

Fabrication and Integration for Multifunctional Epidermal Electronics. A layer of conductive features in the form of mesh heater was created on a SIS substrate. A layer of SIS elastomer was subsequently printed for encapsulation. A second layer of conductive pattern was generated including EMG sensors, electrical stimulators, and interconnects. An additional layer of silicone gel (Silbione RT Gel 4546A/B, Elkem Silicones) was screen printed as the skin adhesive with the electrode area fully exposed. A copper-clad polyimide-based flexible connector was employed to interface with external equipment. Written consent was obtained from all human subjects participated in this study. After cleansing the skin with medical alcohol, the as-prepared multifunctional device was attached to the forearm with sensing electrodes mounted on the right flexor carpi radialis. The electrode–skin impedance was measured by using a GW Instek LCR 6300 meter. A baseline based on commercial Ag/AgCl gel electrodes (2223CN, 3M Co.) was established for comparison. The raw EMG signals were band-pass filtered from 10 to 500 Hz and then recorded at a sampling rate of 20 kHz by using an Intan RHD USB interface board. A Keithley 2634B digital source meter generated monophasic square voltage pulses for electrical stimulation (duration = 4 ms, amplitude = 1 V, frequency = 10 Hz). A DC voltage source (HY3005ET, Hangzhou Huayi Electronics Industry Co., Ltd.) was employed to power the heater. The surface temperature distribution was obtained by using a Testo 885-2 thermal imaging camera through noncontact measurement.

Data, Materials, and Software Availability. All study data are included in the article and/or supporting information.

ACKNOWLEDGMENTS. We acknowledge the support from the National Key Research and Development Program of China (Grant No. 2022YFA1405000), the Natural Science Foundation of Jiangsu Province, Major Project (Grant No. BK20212004), the Key Research and Development Program of Jiangsu Provincial Department of Science and Technology of China (Grant No. BE2019002), the High-Level Entrepreneurial and Innovative Talents Program of Jiangsu Province, and the Program B for Outstanding PhD Candidate of Nanjing University.

1. Z. Cui, Printing practice for the fabrication of flexible and stretchable electronics. *Sci. China Technol. Sci.* **62**, 224–232 (2019).
2. D. J. Lipomi, Z. Bao, Stretchable and ultraflexible organic electronics. *MRS Bull.* **42**, 93–97 (2017).
3. Y. Sun, J. A. Rogers, Inorganic semiconductors for flexible electronics. *Adv. Mater.* **19**, 1897–1916 (2007).
4. S.-T. Han *et al.*, An overview of the development of flexible sensors. *Adv. Mater.* **29**, 1700375 (2017).
5. J. A. Rogers, T. Someya, Y. Huang, Materials and mechanics for stretchable electronics. *Science* **327**, 1603–1607 (2010).
6. A. Chortos, J. Liu, Z. Bao, Pursuing prosthetic electronic skin. *Nat. Mater.* **15**, 937–950 (2016).
7. J. Kim *et al.*, Stretchable silicon nanoribbon electronics for skin prosthesis. *Nat. Commun.* **5**, 5747 (2014).
8. U. Chung Ha *et al.*, Binodal, wireless epidermal electronic systems with in-sensor analytics for neonatal intensive care. *Science* **363**, eaau0780 (2019).
9. H. Lee *et al.*, A graphene-based electrochemical device with thermoresponsive microneedles for diabetes monitoring and therapy. *Nat. Nanotechnol.* **11**, 566–572 (2016).
10. S. Wang *et al.*, Intrinsically stretchable electronics with ultrahigh deformability to monitor dynamically moving organs. *Sci. Adv.* **8**, eabl5511 (2022).
11. J.-W. Jeong *et al.*, Materials and optimized designs for human-machine interfaces via epidermal electronics. *Adv. Mater.* **25**, 6839–6846 (2013).
12. M. Wang *et al.*, Gesture recognition using a bioinspired learning architecture that integrates visual data with somatosensory data from stretchable sensors. *Nat. Electron.* **3**, 563–570 (2020).
13. N. Matsuhisa, X. Chen, Z. Bao, T. Someya, Materials and structural designs of stretchable conductors. *Chem. Soc. Rev.* **48**, 2946–2966 (2019).
14. J. Vanfleteren *et al.*, Printed circuit board technology inspired stretchable circuits. *MRS Bull.* **37**, 254–260 (2012).
15. J. Kang, J. B. H. Tok, Z. Bao, Self-healing soft electronics. *Nat. Electron.* **2**, 144–150 (2019).
16. C. S. Luo, P. Wan, H. Yang, S. A. A. Shah, X. Chen, Healable transparent electronic devices. *Adv. Funct. Mater.* **27**, 1606339 (2017).
17. D. Son *et al.*, An integrated self-healable electronic skin system fabricated via dynamic reconstruction of a nanostructured conducting network. *Nat. Nanotechnol.* **13**, 1057–1065 (2018).
18. B. C. K. Tee, C. Wang, R. Allen, Z. Bao, An electrically and mechanically self-healing composite with pressure- and flexion-sensitive properties for electronic skin applications. *Nat. Nanotechnol.* **7**, 825–832 (2012).
19. P. Song, H. Qin, H.-L. Gao, H.-P. Cong, S.-H. Yu, Self-healing and superstretchable conductors from hierarchical nanowire assemblies. *Nat. Commun.* **9**, 2786 (2018).
20. S. J. Benight, C. Wang, J. B. H. Tok, Z. Bao, Stretchable and self-healing polymers and devices for electronic skin. *Prog. Polym. Sci.* **38**, 1961–1977 (2013).
21. S. A. Odom *et al.*, A self-healing conductive ink. *Adv. Mater.* **24**, 2578–2581 (2012).
22. J. F. Patrick, M. J. Robb, N. R. Sottos, J. S. Moore, S. R. White, Polymers with autonomous life-cycle control. *Nature* **540**, 363–370 (2016).
23. M. D. Dickey, Stretchable and soft electronics using liquid metals. *Adv. Mater.* **29**, 1606425 (2017).
24. S. Handschuh-Wang, F. Stadler, X. Zhou, Critical review on the physical properties of gallium-based liquid metals and selected pathways for their alteration. *J. Phys. Chem. C* **125**, 20113–20142 (2021).
25. N. Kazem, T. Hellebrekers, C. Majidi, Soft multifunctional composites and emulsions with liquid metals. *Adv. Mater.* **29**, 1605985 (2017).
26. S. Chen, H.-Z. Wang, R.-Q. Zhao, W. Rao, J. Liu, Liquid metal composites. *Matter* **2**, 1446–1480 (2020).
27. J. Yan *et al.*, Solution processable liquid metal nanodroplets by surface-initiated atom transfer radical polymerization. *Nat. Nanotechnol.* **14**, 684–690 (2019).
28. J. W. Boley, E. L. White, R. K. Kramer, Mechanically sintered gallium-indium nanoparticles. *Adv. Mater.* **27**, 2355–2360 (2015).
29. J. N. Hohman *et al.*, Directing substrate morphology via self-assembly: Ligand-mediated scission of gallium-indium microspheres to the nanoscale. *Nano Lett.* **11**, 5104–5110 (2011).
30. E. J. Markvicka, M. D. Bartlett, X. Huang, C. Majidi, An autonomously electrically self-healing liquid metal–elastomer composite for robust soft-matter robotics and electronics. *Nat. Mater.* **17**, 618–624 (2018).
31. B. J. Blaiszik *et al.*, Autonomic restoration of electrical conductivity. *Adv. Mater.* **24**, 398–401 (2012).
32. J. Wang *et al.*, Printable superelastic conductors with extreme stretchability and robust cycling endurance enabled by liquid-metal particles. *Adv. Mater.* **30**, 1706157 (2018).
33. L. Mou *et al.*, Highly stretchable and biocompatible liquid metal-elastomer conductors for self-healing electronics. *Small* **16**, 2005336 (2020).
34. M. G. Saborio *et al.*, Liquid metal droplet and graphene co-fillers for electrically conductive flexible composites. *Small* **16**, 1903753 (2020).
35. K. Parida *et al.*, Extremely stretchable and self-healing conductor based on thermoplastic elastomer for all-three-dimensional printed triboelectric nanogenerator. *Nat. Commun.* **10**, 2158 (2019).
36. K. Chu *et al.*, Smart passivation materials with a liquid metal microcapsule as self-healing conductors for sustainable and flexible perovskite solar cells. *Adv. Funct. Mater.* **28**, 1800110 (2018).
37. C. T. Sun, Z. H. Jin, "Chapter 10–Special topics" in *Fracture Mechanics*, C. T. Sun, Z. H. Jin, Eds. (Academic Press, Boston, 2012), pp. 247–285.
38. B. Li *et al.*, Survival and activation behavior of microcapsules in self-healing asphalt mixture. *Constr. Build. Mater.* **260**, 119719 (2020).
39. S. Chen, X. Yang, Y. Cui, J. Liu, Self-growing and serpentine locomotion of liquid metal induced by copper ions. *ACS Appl. Mater. Interfaces* **10**, 22889–22895 (2018).
40. R. David, N. Miki, Synthesis of sub-micrometer biphasic Au–AuGa2/liquid metal frameworks. *Nanoscale* **11**, 21419–21432 (2019).
41. C. J. Thrasher, Z. J. Farrell, N. J. Morris, C. L. Willey, C. E. Tabor, Mechanoresponsive polymerized liquid metal networks. *Adv. Mater.* **31**, 1903864 (2019).
42. J. Y. Chung, J.-H. Lee, K. L. Beers, C. M. Stafford, Stiffness, strength, and ductility of nanoscale thin films and membranes: A combined wrinkling-cracking methodology. *Nano Lett.* **11**, 3361–3365 (2011).
43. J.-H. Pu *et al.*, A strain localization directed crack control strategy for designing MXene-based customizable sensitivity and sensing range strain sensors for full-range human motion monitoring. *Nano Energy* **74**, 104814 (2020).
44. L. Tang, L. Mou, W. Zhang, X. Jiang, Large-scale fabrication of highly elastic conductors on a broad range of surfaces. *ACS Appl. Mater. Interfaces* **11**, 7138–7147 (2019).
45. F. Lawrenz *et al.*, Morphology, mechanical stability, and protective properties of ultrathin gallium oxide coatings. *Langmuir* **31**, 5836–5842 (2015).
46. A. Uppal *et al.*, Pressure-activated thermal transport via oxide shell rupture in liquid metal capsule beds. *ACS Appl. Mater. Interfaces* **12**, 2625–2633 (2020).
47. M. V. Hurley, L. M. Bearne, Non-exercise physical therapies for musculoskeletal conditions. *Best Pract. Res. Clin. Rheum.* **22**, 419–433 (2008).
48. P. Sarzi-Puttini *et al.*, Osteoarthritis: An overview of the disease and its treatment strategies. *Semin. Arthritis Rheum.* **35**, 1–10 (2005).
49. S. Lim *et al.*, Transparent and stretchable interactive human machine interface based on patterned graphene heterostructures. *Adv. Funct. Mater.* **25**, 375–383 (2015).
50. H. Zhu *et al.*, Fully solution processed liquid metal features as highly conductive and ultrastretchable conductors. *npj Flexible. Electron.* **5**, 25 (2021).